

RADIATIVE TRANSFER PROBLEM IN DUSTY GALAXIES: EFFECTS OF NON-ISOTROPIC MULTIPLE SCATTERING

D. Semionov and V. Vansevicius

Institute of Physics, Savanorių 231, Vilnius LT-02300, Lithuania

Received 2005 April 5; revised 2005 May 24

Abstract. We investigate the effects of multiple anisotropic light scattering by interstellar dust particles on photometric profiles of disk galaxy models computed using an iterative ray-tracing radiative transfer modeling code. It is shown that anisotropic scattering must be fully accounted for in at least the first scattering event for all considered cases. At the same time scattering terms of the order higher than 5th can be safely approximated using the isotropic phase function. The effects of isotropic approximation are most significant in the galaxy models seen face-on with dust population extending beyond the stellar disk, therefore the applicability of isotropic approximation to a higher-order (2 to 5) scattering terms depends on the assumed galaxy model parameters, namely, the optical depth, scattering albedo and the distribution of interstellar dust with respect to stars.

Key words: radiative transfer – ISM: dust, extinction.

1. INTRODUCTION

Optical interstellar dust grain properties still remain an uncertain factor in our understanding of star formation history in galaxies. Existing models and theories of interstellar dust are primarily intended to describe the optical properties of grains by means of size, composition and relative abundance of different grain types, with limited connection to the general chemical evolution of interstellar matter (ISM) (Li & Greenberg 2003). At the same time, observations of the Milky Way and external galaxies reveal a multitude of existing extinction laws and relative distributions of stellar populations and ISM. A straightforward attempt to reproduce full complexity of the processes in ISM in order to model the observed galactic spectral energy distribution (SED) introduces a large number of free parameters, resulting in a significantly degenerate solution (e.g., Silva et al. 1998). Considering the difficulty of practical and theoretical determination of the optical properties and the lack of the unified theory of ISM, an attempt to analyze a simplified model to discern relative influence of stellar and dust content and their distribution might prove to be fruitful (e.g., Ferrara et al. 1999).

A canonical formulation of the radiative transfer (RT) problem in the form (Chandrasekhar 1960)

$$\frac{dI_\lambda}{ds} = -\kappa_\lambda I_\lambda + j_\lambda + \kappa_\lambda \frac{\omega_\lambda}{4\pi} \int I_\lambda \Phi_\lambda(\Omega) d\Omega, \quad (1)$$

defines three main optical properties of intervening matter: extinction mass coefficient κ_λ , scattering albedo ω_λ and scattering phase function Φ , commonly described by means of phase function parameter g_λ (Henyey & Greenstein 1941). While the values of the first two parameters might be obtained from the total emissivity, the absorbed (and re-radiated) energy and the observed SED, the determination of phase function anisotropy is less certain and usually depends on assumptions about structure, chemical composition and size distribution of interstellar dust grains.

In this paper we attempt to estimate the influence of scattering phase function anisotropy on the SEDs of model disk galaxies. The description of the RT code, used to compute model SEDs, and the assumed galaxy model parameters are presented in Section 2. The results, obtained using the isotropic approximation are compared with those from fully anisotropic calculations in Section 3. In the same section we discuss isotropic approximation applicability limits.

2. MODELS AND METHODS

To test the influence of the anisotropic scattering phase function, the RT problem has been solved for the six pure disk galaxy model families S1–S6 with varying relative star and dust distributions. Both stars and dust are assumed to have double-exponential distribution of luminosity and mass, respectively:

$$\rho(r, z) = \rho_0 \exp\left(-\frac{r}{r_{\text{eff}}} - \frac{|z|}{z_{\text{eff}}}\right), \quad (2)$$

r_{eff} and z_{eff} being the effective scale-length and scale-height for the appropriate distribution. The common effective scale-length of stellar and dust distribution was assumed to be constant, while the effective scale-height of dust distribution z_{eff}^d was varied with respect to the effective scale-height of stellar disk to represent three commonly used cases – “dust within stellar disk” ($z_{\text{eff}}^d = 0.5z_{\text{eff}}$, models S1 and S4), “well-mixed dust and stars” ($z_{\text{eff}}^d = z_{\text{eff}}$, models S2 and S5) and “dust enveloping stellar disk” ($z_{\text{eff}}^d = 2z_{\text{eff}}$, models S3 and S6). We have used two values of total dust mass, corresponding to the optical depth to the model center in V passband, measured perpendicularly to the disk plane: $\tau_V = 1$ for models S1–S3 and 10 for models S4–S6.

Table 1. Galaxy model parameters.

	S1	S2	S3	S4	S5	S6
$z_{\text{eff}}^d/z_{\text{eff}}$	0.5	1	2	0.5	1	2
τ_V	1	1	1	10	10	10

Each model family in S1–S6 contains a sequence of five models computed with eight scattering iterations and denoted M0:8, M1:7, M3:5, M5:3 and M8:0, with first and second digits in the model name corresponding to the number of initial anisotropic and subsequent isotropic iterations respectively (e.g., M0:8 being computed with fully isotropic scattering, M1:7 has first iteration computed with anisotropic scattering and following seven iterations using isotropic approximation, etc.).

Optical dust grain properties, shown in Figure 1, were computed using the Laor & Draine (1993) model, approximating the Milky Way galaxy type extinction using a mixture of graphite and silicate grains in the proportion of 0.47 to 0.53, with grain size distribution following the power law $a^{-3.5}$ with lower and upper cut-off

radii $a_{\min} = 0.005 \mu\text{m}$ and $a_{\max} = 0.25 \mu\text{m}$. SEDs of the models were computed using the Galactic Fog Engine RT code (GFE, Semionov & Vansevicius 2002; Semionov 2003; Semionov & Vansevicius 2005), implementing an iterative 2-D ray-tracing algorithm in axisymmetrical geometry. The galaxy model is represented as a cylinder, divided into 20 layers consisting of 25 concentric rings, truncated at the radius $r_{\max} = 6r_{\text{eff}}$ and the height above and below the disk central plane $z_{\max} = \pm 6z_{\text{eff}}$. The GFE uses a static ray-casting scheme to produce a sufficient sampling of the galaxy model by a set of rays, and then solves 1-D RT problem (Eq. 1) along each ray. During the first iteration the initial global radiation field of the system, I_0 , determined from the stellar luminosity distribution, contributes to the escaped energy (the observed SED), the absorbed energy E_{λ}^{abs} and the global radiation field of once-scattered light, I_1 . Higher-order (i th) scattering events are accounted for by substituting I_{i-1} as input to calculate I_i and accumulating obtained escaped and absorbed energy in subsequent iterations.

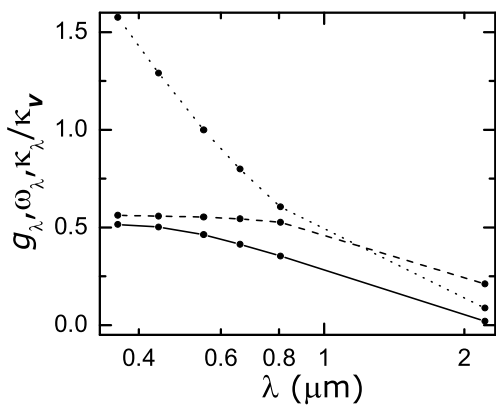


Fig. 1. Assumed optical properties of interstellar grains. Solid, dashed and dotted lines show the scattering phase function parameter g_{λ} , albedo ω_{λ} and relative mass extinction coefficient $\kappa_{\lambda}/\kappa_V$, respectively. Dots show positions of the U , B , V , R , I and K passbands.

For all model families we have computed images with a scale of $0.1z_{\text{eff}}$ per pixel at the wavelengths corresponding to the U , B , V , R , I and K passbands for model galaxy inclinations of 0° , 50° , 80° and 90° . To investigate the differences in the observed quantities of galaxy models we performed surface photometry of these images using apertures with ellipticity determined from the model inclination, the aperture being centered on the geometric center of the model galaxy image, obtaining differential azimuthally-averaged color excess profiles. The example of the color excess E_{V-K} photometric profiles for the galaxy models M8:0, computed with fully anisotropic scattering, is shown in Figure 3 as a function of the aperture semi-major axis radius given in units of r_{eff} . Since the observed minor axis cross-sections of galaxies are more frequently available than multiaperture photometry or complete photometric profiles and are widely used in determination of

For all models at all considered wavelengths the amount of total radiative energy, remaining to be scattered after the 8th iteration, and a total energy defect due to numerical inaccuracies were found to be below 0.5% and 1% of total emitted energy, E_{λ}^{tot} , respectively. The resulting attenuation curves (the ratio of the flux “observed” from the dusty model galaxy to the flux from the dust-free model galaxy), $A(\lambda) = F_7(\lambda)/F_0(\lambda)$, and the spectral distribution of the normalized absorbed energy (the ratio of the absorbed energy to the total emitted energy), $E_{\lambda}^{\text{abs}}/E_{\lambda}^{\text{tot}}$, are shown in Figure 2. We have found, that the total amount of the absorbed energy in model galaxies E_{λ}^{abs} only slightly depends on g_{λ} , varying within 2% of E_{λ}^{tot} for all considered cases and thus cannot indicate the effect of anisotropic scattering.

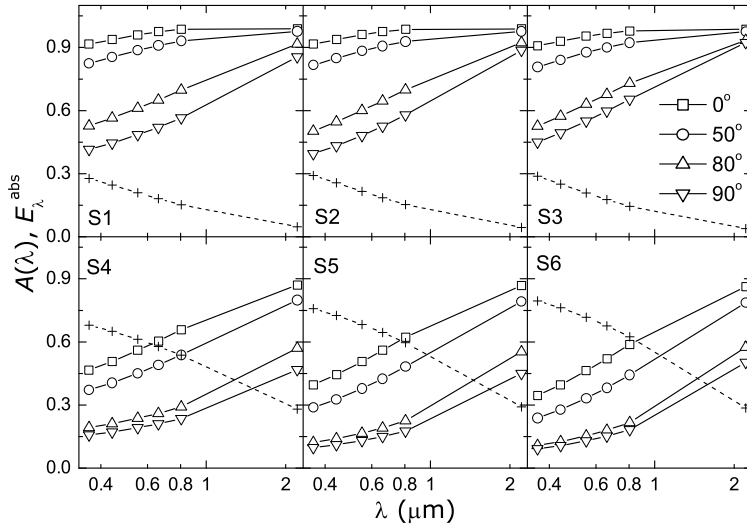


Fig. 2. Attenuation curves and absorbed energy for the models S1–S6. Solid lines show attenuation curves for model galaxies with inclinations of 0° , 50° , 80° and 90° , the dotted line shows the normalized absorbed energy.

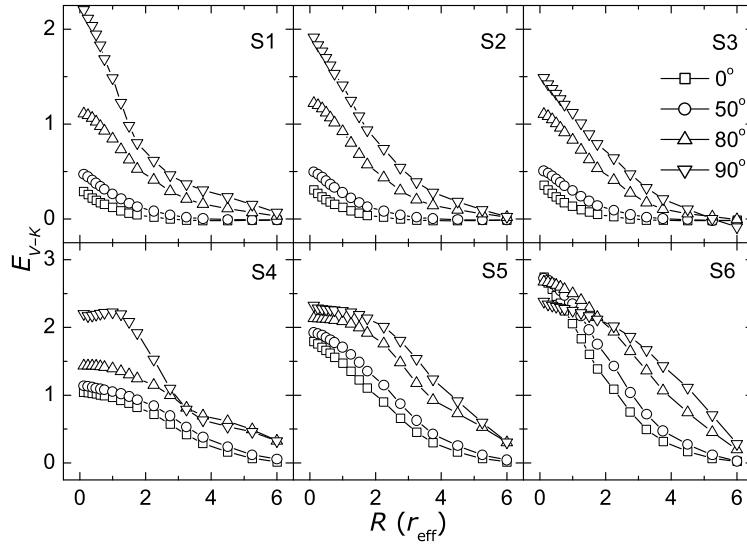


Fig. 3. Photometric profile of color excess E_{V-K} for the model groups S1–S6. Lines correspond to the model galaxy inclinations of 0° , 50° , 80° and 90° . The aperture semi-major axis radius is given in units of the effective stellar disk scale-length r_{eff} .

the effective scale-lengths and scale-heights of stellar populations and extinction distribution, we have extracted from the images color excess profiles along their minor axes. Hereafter we will use differences of photometric profiles and minor axis cross-sections (denoted by a “*C*” superscript) between the fully anisotropic models M8:0 on one side and the models computed using varying levels of isotropic approximation: M0:8, M1:7, M3:5 and M5:3, on other side. For example, in the case of E_{V-K} we have

$$\Delta E_{V-K}^{Mi} = E_{V-K}^{M8:0} - E_{V-K}^{Mi}. \quad (3)$$

3. RESULTS AND DISCUSSION

The results obtained allow us to distinguish two model groups according to their effective opacity: the low opacity models S1–S4 and the high opacity models S5 and S6. Models in the group S1–S4 display similar isotropic approximation-induced error distributions and their absolute values for most of the performed tests, while models S5 and S6 appear significantly different and have to be considered separately.

The effects of anisotropic scattering on the photometric profile of color excess, as shown in Figure 4 for E_{V-K} , are the most prominent for the models S5 and S6 seen face-on. The central values of color excess appear to be overestimated for all models computed with any level of isotropic scattering approximation. The model group S1–S4 shows acceptable accuracy starting from the M1:7 models, approximated solutions significantly deviate from fully anisotropic cases only at high inclination, where it would be necessary to apply anisotropic treatment up to the first three iterations.

Differences of color excesses of the minor axis cross-sections, ΔE_{B-V}^C , ΔE_{V-I}^C and ΔE_{V-K}^C , computed for the models with isotropic approximation from one side and for the models with anisotropic scattering phase function on other side, are shown in Figures 5–7. The deviations in E_{U-V}^C and E_{V-R}^C being identical to ΔE_{B-V}^C and ΔE_{V-I}^C in form, differ from them only by absolute values. Similarly to the results, obtained for azimuthally-averaged photometric profiles, two model groups can be distinguished, low opacity group S1–S4 and high opacity group S5–S6. Galaxy models in the S1–S4 group computed assuming the isotropic scattering in most cases display small deviations from the fully anisotropic M8:0 models, mostly concentrated near the image center. In contrast, the model group S5–S6 shows large errors at all inclinations, affecting significant part of the minor axis cross-sections, thus requiring at least three (in some cases up to five) first iterations to fully account for the scattering anisotropy.

As can be seen in Figures 4–7, the purely isotropic models provide a poor approximation to the solutions obtained with appropriate values of g_λ . The M1:7 approximation offers an improvement by a factor of 2 or more over M0:8 in reproducing photometric profiles of models in the S1–S4 group, while for the model families S5 and S6 the improvement shown by model M1:7 in respect to M0:8 is less prominent. In general, the M3:5 models produce the results that with acceptable tolerance can be considered identical to fully anisotropic models. Isotropic approximation in the 6th and subsequent iterations does not introduce a significant error since these iterations contribute only minor fraction to the energy balance.

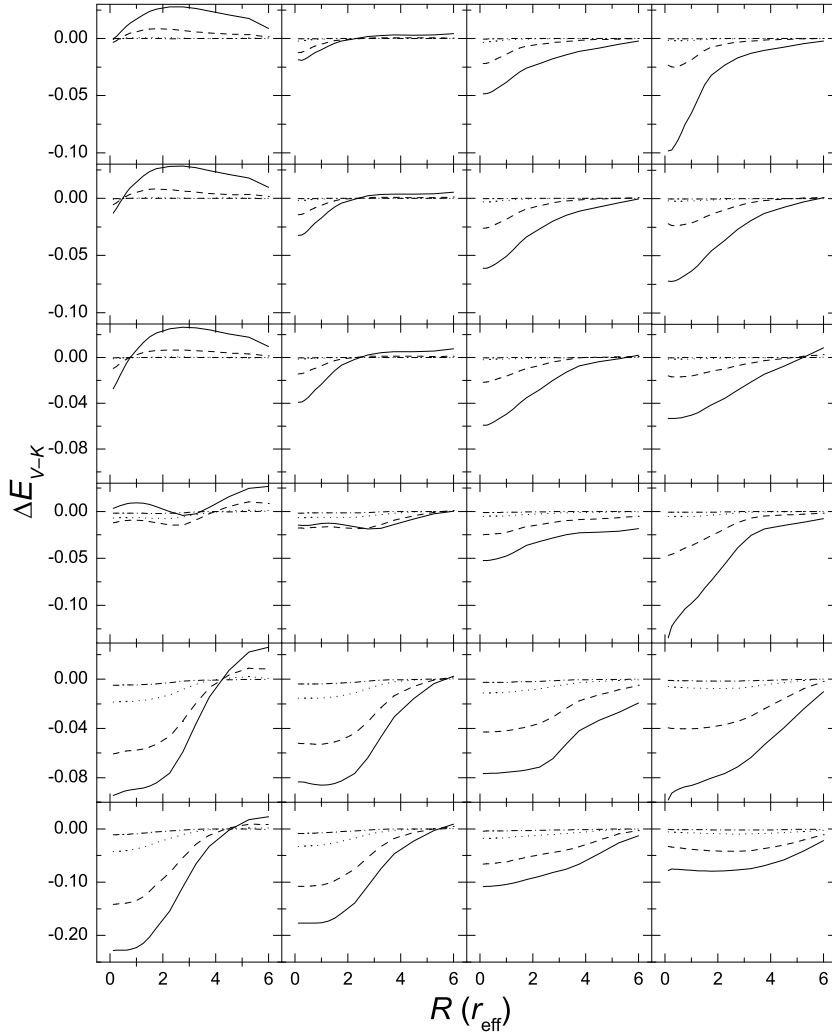


Fig. 4. Differences in E_{V-K} photometric profile between disk galaxy models computed with isotropic and anisotropic scattering. Panel rows correspond to the models S1–S6 (starting from top), panel columns – to model inclinations of 0° , 50° , 80° and 90° (left to right). Solid, dashed, dotted and dash-dotted lines correspond to differences between the M8:0 model from one side and the M0:8, M1:7, M3:5 and M5:3 models from other side. The aperture semi-major axis radius is given in units of the effective stellar disk scale-length r_{eff} .

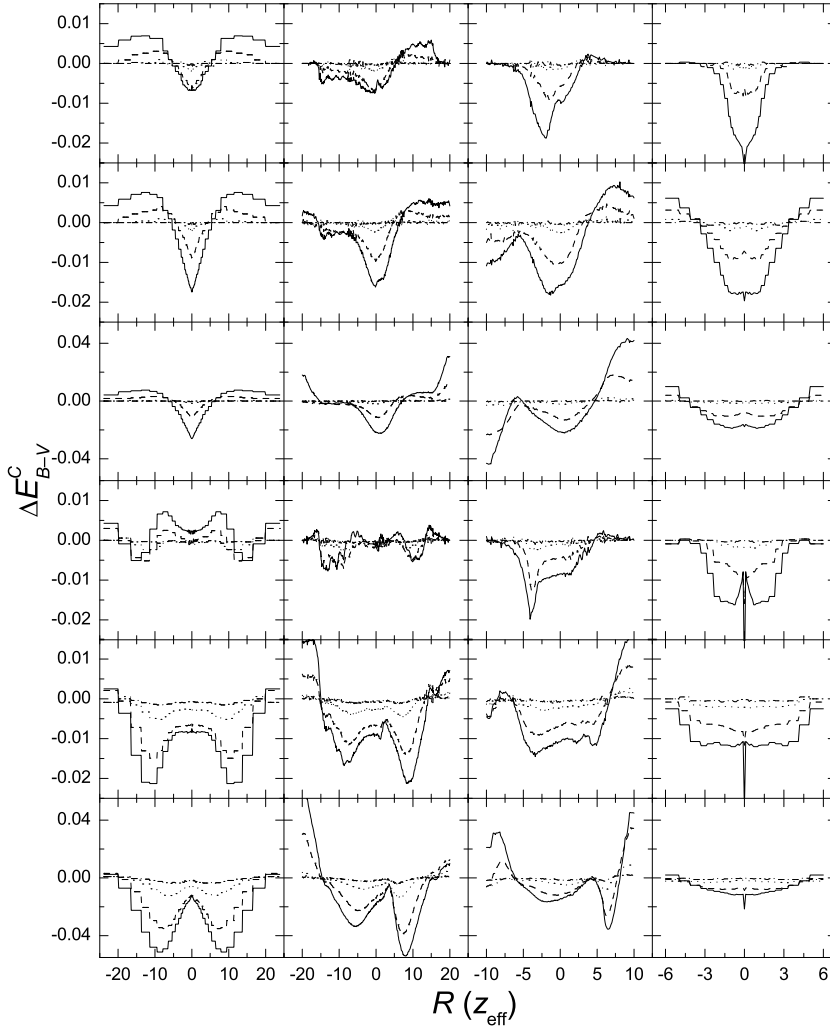


Fig. 5. Differences in E_{B-V} minor axis cross-section between disk galaxy models computed with isotropic and anisotropic scattering. Panel rows correspond to models S1–S6 (starting from top), panel columns – to model inclinations of 0° , 50° , 80° and 90° (left to right). Solid, dashed, dotted and dash-dotted lines correspond to differences between the M8:0 model from one side and the M0:8, M1:7, M3:5 and M5:3 models from other side. The distance from the model galaxy image center is given in units of the effective stellar disk scale-height z_{eff} , negative R values correspond to half of the model closer to the observer.

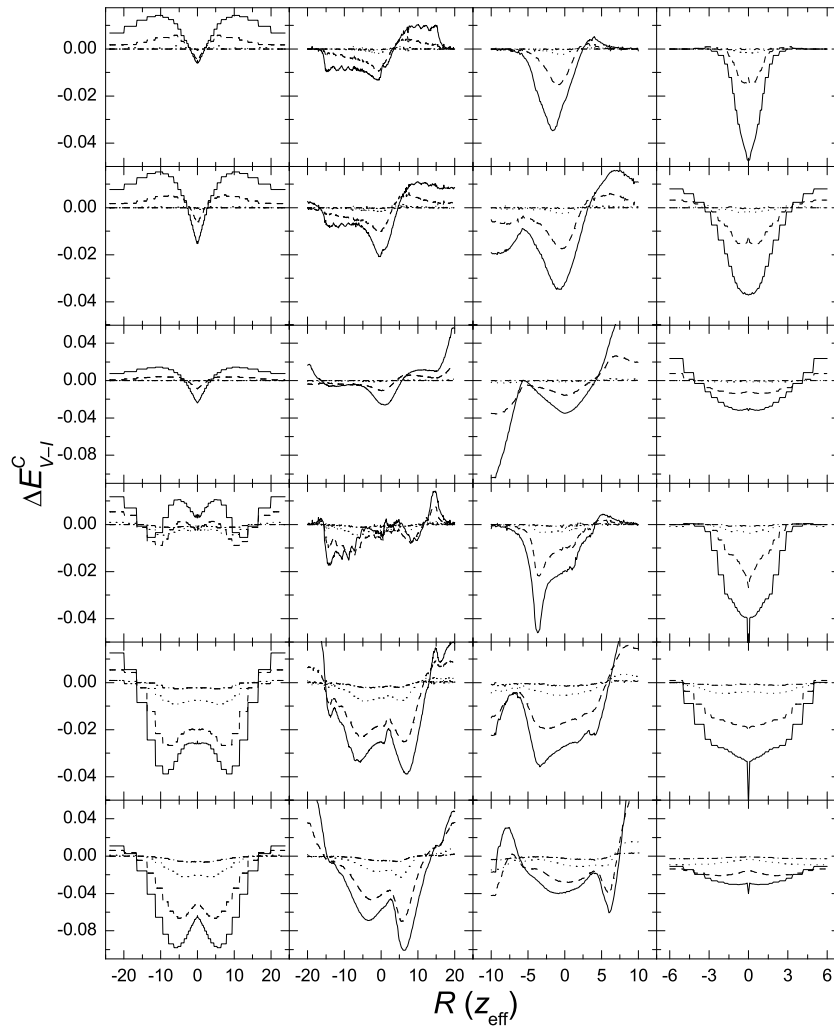


Fig. 6. The same as in Fig. 5, but for E_{V-I} minor axis cross-section.

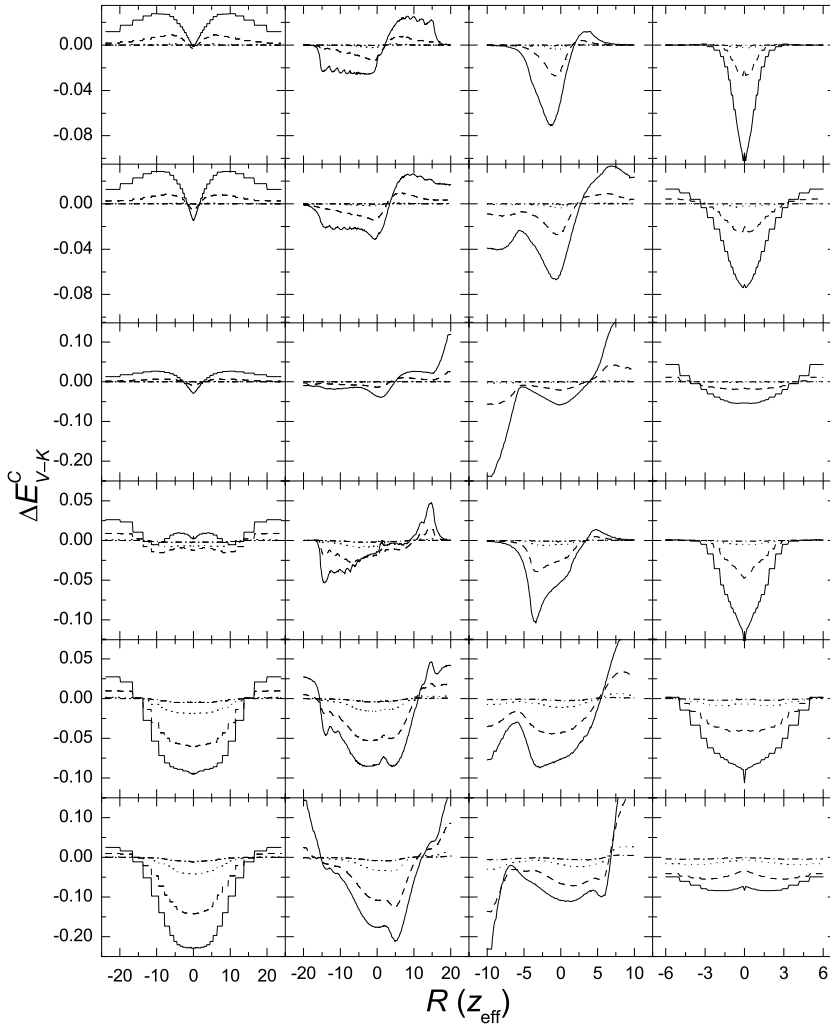


Fig. 7. The same as in Fig. 5, but for E_{V-K} minor axis cross-section.

However, when comparing the relative differences between models M1:7, M3:5 and M5:3, it is necessary to take into account both the required numerical accuracy and the computational efficiency of the code.

Approximation of some iterations using the isotropic phase function has a potential to improve the performance of RT problem-solving code by reducing computing time and memory requirements. For Monte-Carlo based methods such approximation will allow use of more efficient algorithms as well as decrease resources necessary to follow individual photons through the model. For the iterative RT problem-solving algorithms, such as ray-tracing based code used in this work, the isotropic approximation also significantly speeds up calculations and improves code's accuracy, since it eliminates numerical errors caused by otherwise necessary interpolation of the scattering phase function.

4. CONCLUSIONS

We have presented a study of the effect of isotropic scattering phase function approximation on photometric properties of the model disk galaxies having several commonly assumed star and dust relative distributions. It has been shown that in all cases it is necessary to fully take into account the anisotropic scattering in at least the first scattering event. The subsequent scatterings can be assumed to be isotropic with varying degree of accuracy depending on the model extinction distribution. The effect of anisotropic scattering in terms of higher than 5th order is negligible since their contributions to the overall energy balance of the model is small. The largest errors in the extinction and color excess profiles and the minor axis cross-sections, caused by isotropic approximation, were found for the models with dust distribution being more extended than the stars, while models with the extinction concentrated at the disk midplane are least affected by the isotropic scattering approximation. It was found that the effect of isotropic approximation of scattering phase function on the color excess photometric profiles and the minor axis cross-sections depends strongly on the difference in g_λ of the involved photometric passbands, while the effect of the difference in the relative extinction τ_λ/τ_V is marginal.

ACKNOWLEDGMENT. This work has been supported by the Lithuanian State Science and Studies Foundation.

REFERENCES

- Chandrasekhar S. 1960, *Radiative Transfer*, New York, Dover
 Ferrara A., Bianchi S., Cimatti A., Giovanardi C. 1999, ApJS, 123, 427
 Henyey L., Greenstein J. 1941, ApJ, 93, 70
 Laor A., Draine B. 1993, ApJ, 402, 441
 Li A., Greenberg M. 2003, in *Solid State Astrochemistry*, eds. V. Pirronello, J. Krelowski & G. Manicò, Kluwer Academic Publishers, Dordrecht, p. 37
 Semionov D., Vansevičius V. 2002, Baltic Astronomy, 11, 537
 Semionov D. 2003, *Spectrophotometric Evolution of Dusty Disk Galaxies*, Inst. of Theoretical Physics and Astronomy, Vilnius, PhD thesis
 Semionov D., Vansevičius V. 2005, astro-ph/0501146
 Silva L., Granato G., Bressan A., Danese L. 1998, ApJ, 509, 103